JCI The Journal of Clinical Investigation

Peanut oral immunotherapy differentially suppresses clonally distinct subsets of T helper cells

Brinda Monian, … , Wayne G. Shreffler, J. Christopher Love

J Clin Invest. 2021. https://doi.org/10.1172/JCI150634.

Research In-Press Preview Immunology

Graphical abstract

Peanut oral immunotherapy differentially suppresses clonally distinct subsets of T helper cells

Author List: Brinda Monian[1,2,*], Ang A. Tu[1,3,*], Bert Ruiter[4,5], Duncan M. Morgan[1,3], Patrick M. Petrossian[1], Neal P. Smith[4,5], Todd M. Gierahn[1], Julia H. Ginder[1], Wayne G. Shreffler[4,5,**], J. Christopher Love[1,2,6,**]

Author Affiliations:

[1]Koch Institute for Integrative Cancer Research, Massachusetts Institute of Technology, Cambridge, MA, USA

[2]Department of Chemical Engineering, MIT, Cambridge, MA, USA

[3]Department of Biological Engineering, MIT, Cambridge, MA, USA

[4]Center for Immunology and Inflammatory Diseases, Massachusetts General Hospital, Boston, MA, USA

[5]Harvard Medical School, Boston, MA, USA

[6]Broad Institute of MIT and Harvard, Cambridge, MA, USA

*These authors contributed equally.

**These authors contributed equally.

Corresponding Authors:

Wayne G. Shreffler

Massachusetts General Hospital

Charlestown Navy Yard Building 149

Mailstop CNY 149-8, 149 13th Street

Boston, MA 02129

Phone: 617-726-6147

Email: wshreffler@mgh.harvard.edu

J. Christopher Love

Massachusetts Institute of Technology

77 Massachusetts Avenue, Building 76-253

Cambridge, MA 02139

Phone: 617-234-2300

Email: clove@mit.edu

Abstract

Food allergy affects an estimated 8% of children in the US. Oral immunotherapy (OIT) is a recently approved treatment, with outcomes ranging from sustained tolerance to food allergen to no apparent benefit. The immunological underpinnings that influence clinical outcomes of OIT still remain largely unresolved. Using single-cell RNA sequencing and paired TCRα/β sequencing, we assessed the transcriptomes of CD154+ and CD137+ peanut-reactive T helper cells from 12 peanut-allergic patients longitudinally throughout OIT. We observed expanded populations of cells expressing Th1, Th2, and Th17 signatures that further separated into six clonally distinct subsets. Four of these subsets demonstrated convergence of TCR sequences, suggesting antigen-driven T cell fate. Over the course of OIT, we observed suppression of Th2 and Th1 gene signatures in effector clonotypes but not Tfh-like clonotypes. Positive outcomes were associated with stronger suppression of Th2 signatures in Th2A-like cells, while treatment failure was associated with the expression of baseline inflammatory gene signatures that were present in Th1 and Th17 populations and unmodulated by OIT. These results demonstrate that differential clinical responses to OIT are associated both with pre-existing characteristics of peanut-reactive CD4+ T cells and with suppression of a subset of Th2 cells.

Conflict of Interest Statement

A.A.T., T.M.G., J.C.L., and the Massachusetts Institute of Technology have filed patents related to the single-cell sequencing methods used in this work. J.C.L. has interests in Sunflower Therapeutics PBC, Pfizer, Honeycomb Biotechnologies, OneCyte Biotechnologies, SQZ Biotechnologies, Alloy Therapeutics, QuantumCyte, Amgen, and Repligen. J.C.L.'s interests are reviewed and managed under Massachusetts Institute of Technology's policies for potential conflicts of interest. J.C.L. receives sponsored research support at MIT from Amgen, the Bill & Melinda Gates Foundation, Biogen, Pfizer, Roche, Takeda, and Sanofi. The spouse of J.C.L. is an employee of Sunflower Therapeutics PBC. W.G.S. has interests in Aimmune Therapeutics, Allergy Therapeutics, FARE, DBV Biotechnologies, Merck, and Sanofi. W.G.S.'s interests are reviewed and managed under Mass General Brigham's policies for potential conflicts of interest. W.G.S. receives sponsored research support at MGH from Aimmune, DBV, The Demarest Lloyd Foundation, The Food Allergy Science Initiative at the Broad Institute, Regeneron, and Vedanta. T.M.G. is currently an employee of Honeycomb Biotechnologies, Inc. A.A.T. is currently an employee of Immunitas Therapeutics, Inc. B.M. is currently an employee of Generate Biomedicines, Inc.

Introduction

Food allergy is an immune hypersensitivity condition characterized by high-affinity allergen-specific IgE antibodies and allergen-specific Th2 cells (1–3). Specific IgE binds to effector cells, such as mast cells and basophils, through FcεRI receptors that are cross-linked upon binding of allergen. The resulting cellular degranulation causes local and systemic release of histamine and other mediators, leading to allergic reactions ranging from mild symptoms, such as hives and abdominal pain, to potentially life-threatening anaphylaxis (4). Allergen-specific Th2 cells constitute a critical component in this cascade. Th2 cells are broadly defined by the expression of the transcription factor GATA3 and the secretion of cytokines IL-4, IL-5, and IL-13, which promote class-switching of B cells to IgE and the recruitment of other effector cells, such as eosinophils (5, 6). Recent studies have highlighted subtypes of Th2 cells with specialized functions in the context of allergy, including effector memory (e.g. Th2A, peTh2), and T follicular helper (e.g. Tfh13) phenotypes (6–10).

Oral immunotherapy (OIT) is currently the only FDA-approved treatment for food allergy intended to prevent anaphylaxis (11). OIT involves the daily ingestion of escalating doses of allergen. Most patients (80-85%) achieve desensitization (a loss in clinical reactivity with regular consumption of allergen), but only about a third of patients maintain unresponsiveness if treatment is discontinued for even just a few months (12–14). Studies of the impact of OIT on circulating T cells have consistently found evidence for suppression of Th2 responses, but most of these studies have not correlated T cell responses with heterogenous clinical outcomes (7, 15–18). Similarly, while regulatory T cell (Treg) induction has been observed using in vitro expansion of T cells from OIT patients, it has not been consistently shown ex vivo (17–24). Studying allergen-reactive T cell subsets ex vivo is challenging due to their low frequencies in peripheral blood and technical constraints, which limit the ability to phenotype these populations reliably and to track corresponding clonotypes longitudinally (22, 25). As a result, existing data on T cell responses in

93 the context of OIT have been limited to features comprising a narrow set of genes and proteins,
94 or T cells specific for a pre-defined subset of allergen epitopes (17, 22). Comprehensive
95 characterization of allergen-specific CD4+ T cell subsets and their response to immunotherapy
96 over time may not only refine strategies for the treatment of food allergy, but may also enhance
97 our broader understanding of T helper cell phenotypes in atopic disease.
98

Results

Single-cell RNA-Seq enables deep profiling of peanut-reactive T helper cells from OIT patients. To measure the impact of OIT on peanut-reactive T cells, we profiled longitudinal blood samples from 12 patients participating in a clinical trial of peanut OIT (NCT01750879, **Supplementary Tables** 1 and 2). In brief, peripheral blood mononuclear cells (PBMCs) were isolated from each patient at four timepoints: baseline (BL; before therapy), buildup (BU; 13 weeks after start of therapy), maintenance (MN; 12 weeks after the maximum dose was reached), and avoidance (AV; 12 weeks after the end of therapy). Clinical outcomes were evaluated by two oral food challenges and were defined as: tolerance (TO) - passing both food challenges; partial tolerance (PT) - passing the challenge at the maintenance timepoint but failing the challenge at the avoidance timepoint; and treatment failure (TF) - failing the challenge at the maintenance timepoint. Samples from three placebo-treated (PL) patients were also included (**Figure** 1A; **Methods**). Consistent with prior studies, peanut-specific IgE levels demonstrated a transient increase at buildup (20, 26); however, peanut-specific IgE concentrations did not correlate with clinical outcomes at any timepoint (**Supplementary Figure 1**).

To enrich for allergen-specific T cells and capture their activated profiles, we cultured the PBMCs with whole peanut protein extract for 20 hours to activate CD4+ memory T cells. Peanut-reactive cells were then enriched via FACS using CD154 and CD137 (activation markers for effector and regulatory T cell states, respectively) (**Figure** 1, A and B; **Supplementary Figure** 2A) (27–29). This approach allowed us to recover a broad set of peanut-specific T cells with limited bias for specific epitopes or HLA types (29). The 20h stimulation time was intended to capture ex vivo cell states and reflect in vivo clonal distributions; it provides sufficient time for the processing of whole peanut proteins by antigen-presenting cells and the activation of peanut-reactive CD4+ T cells, but it is too short to induce substantial proliferation of antigen-activated T cells (27, 28, 30, 31) . CD154-based approaches have been broadly used to identify antigen-reactive CD4+ T cells in

various contexts (25, 32–34). In addition, we have previously shown that the frequency of peanut-reactive CD154+ CD4+ T cells in peanut-allergic patients is correlated with the patients' clinical sensitivity, illustrating the specificity of this assay (10, 35). Using this method, we observed that OIT significantly decreased the frequency of peanut-reactive CD154+ and CD137+ T cells in the peripheral blood (**Figure** 1C); this trend was not observed in the placebo group (**Supplementary Figure** 2B). The frequency of CD154+ T cells in unstimulated cultures from the same patients was low, indicating that CD154 expression was induced by peanut stimulation and not associated with activated memory T cells already present in the peripheral blood (**Supplementary Figure** 2C).

To further characterize peanut-reactive memory CD4+ T cells and study how their phenotypes and repertoire are altered during OIT in relation to treatment outcome, we processed the sorted cells for single-cell RNA-Seq via Seq-Well and paired single-cell TCRα/β sequencing (36, 37). We also processed CD154-CD137- cells from a subset of patients for use as controls. After filtering cell transcriptomes for library quality, we recovered high-quality transcriptomes for 134,129 cells (**Methods; Supplementary Figure** 3A).

Peanut-reactive T cell transcriptomes formed clusters associated most closely with their sorted subsets (**Figure** 2A). We observed patient-specific variation within each cluster that was not a function of library size or mitochondrial content (**Figure** 2B; **Supplementary Figure** 3), suggesting that it represented inherent biological rather than technical differences. CD154+ and CD137+ cells were separated by many differentially expressed genes, including their associated transcripts *CD40LG* and *TNFRSF9*, the Treg marker *FOXP3*, and others consistent with effector and regulatory phenotypes, respectively (**Figure** 2C). Qualitatively, there was no strong association between transcriptome (as measured by UMAP embeddings) and timepoint or

150 treatment outcome, suggesting that OIT-induced effects might be subtle rather than dominant in
151 the data.
152
153 **Sparse PCA delineates canonical and new T-helper cell gene modules.** To uncover evidence
154 of OIT-driven variation among peanut-reactive T cells, we developed an unsupervised approach
155 to identify conserved programs of immune-related gene expression. The dataset was filtered to
156 937 immune and variable genes (**Supplementary Table** 3). Then, co-expressed genes were
157 aggregated into gene modules using sparse principal components analysis (PCA) (38) to derive
158 a set of 50 gene modules (**Methods**; **Supplementary Figure** 4,5). Several modules
159 corresponded with phenotypes of known T cell subsets, such as Th1, Th2, Th17, and regulatory
160 T cells (**Figure** 2C). 43 out of 50 gene modules were present across most or all patients
161 (**Supplementary Figure** 6; **Methods**), indicating that these represent programs of T cell function
162 or activation that are consistent among individuals.
163
164 **Th-related gene modules are associated with expanded T cells.** To investigate clonal T cell
165 responses to peanut antigens, we recovered paired TCR sequences from single-cell whole
166 transcriptome amplification product. We identified TCRβ sequences for 60% (+/-17%), TCRα for
167 55% (+/-15%) and both chains for 36% of cells (+/- 12%) (numbers represent median +/- standard
168 deviation across patients). Coverage was uniform across samples, and the majority of expanded
169 TCRβ sequences were paired with a single TCRα (**Figure** 3A; **Supplementary Figure** 7). Given
170 this relationship, we used TCRβ for all subsequent analyses involving clonotypes. The diversities
171 of CD154+ and CD137+ repertoires were significantly lower than those of the CD154-CD137-
172 cells, indicating that these activation markers enriched for a pool of clonally expanded, peanut-
173 reactive clonotypes (**Figure** 3, B and C). In addition, we observed that 55% of expanded clones
174 were detected across multiple time points, but only 1.6% of clonotypes were shared between

CD154+ and CD137+ cells, suggesting that these two activated subsets resulted from fundamental differences in lineage, epitope specificity, or both (**Figure** 3D).

To determine which, if any, gene modules were associated with clonal T cell expansion, we classified cells as expressing or non-expressing for each module, based on whether the module score was above background expression in CD154-CD137- cells (**Methods**). We then calculated the average TCRβ clonal size for cells expressing each module, as well as the average score of that module in CD154+ cells relative to CD154-CD137- cells. We found that modules representing Th1, Th2, and Th17 functions exhibited strong upregulation in both the CD154+ and CD137+ compartments and were associated with expanded T cell clonotypes, suggesting that these phenotypes are largely associated with peanut-reactive clonotypes rather than with bystander-activated, non-peanut-reactive T cells (**Figure** 3E; **Supplementary Figure** 8).

Peanut-reactive T helper cells include six phenotypically distinct states. Given their strong enrichment in the CD154+ and CD137+ compartments, we further analyzed the heterogeneity among cells expressing the Th1, Th2, and Th17 modules. Separate clustering of these cells revealed three phenotypically distinct clusters of Th2 cells and two clusters of Th1 cells. We did not observe additional clusters within the Th17 cells (**Figure 4**A). These clusters were detected in all patients (**Supplementary Figure** 9). Within the Th2 cells, the clusters corresponded to a Tfh2-like population (high in costimulatory markers, *CXCR5*, and *PDCD1*), a Th2reg-like population (*FOXP3* and *TNFRSF9*), and a Th2A-like population (7, 39) (*GATA3*, *IL17RB*, and *PTGDR2*; **Figure** 4D). The Tfh2-like population resembled a previously-described pathogenic Tfh13 subset, while the Th2A-like population shared markers previously identified in Th2A and peTh2 populations (7–9) (**Supplementary Figure** 10). Likewise, the Th2reg-like population shared features with previously described deviated Treg cells in food allergy (40). Among the Th1 cells, the clusters corresponded to a Tfh1-like population and a Th1-conv (conventional)

population with canonical Th1 signatures (41) (**Figure 4,** A and D)**.** Both of these clusters expressed high levels of *IFNG* and *GZMB*, and the Tfh1-like cluster exhibited high overlap of genes also expressed in the Tfh2-like population, including *ICOS*, *PDCD1* and *TNFRSF9*.

We hypothesized that Tfh2-like cells influence the class-switching of peanut-specific B cells to IgE. To investigate this hypothesis, we determined the correlation between the average expression of each gene expressed by Tfh2-like cells and peanut-specific IgE titer for each patient at each timepoint. In total, we detected 66 genes that were significantly correlated with peanut-specific IgE levels in plasma (**Supplementary Figure** 11). Transcripts positively correlated with IgE included the Th2 cytokines *IL5* and *IL4*; this correlation was observed in Tfh2-like but not Th2A-like cells (**Figure** 4B). Other positive correlates with IgE included the costimulatory receptor *ICOS*, the gut homing integrin *ITGA4*, and *PLA2G16* and *GK*, two transcripts implicated in the production of prostaglandin-D2 by peTh2 cells in eosinophilic esophagitis (42), while transcripts negatively correlated with IgE production included *TGFB1*, which is associated with class-switching to IgA (43, 44), and *TNFSF10*, which has been demonstrated to dampen Th2 responses in allergic asthma (45) (**Supplementary Figure** 11). No genes expressed by Th2A-like cells were significantly correlated with peanut-specific IgE. These results demonstrate a relationship between gene expression in Tfh2-like cells and peanut-specific IgE levels and suggest that cytokine signals from different Th2 subsets may contribute differently to class-switching to IgE.

Peanut-reactive T helper cell phenotypes are clonally distinct. We next sought to determine the clonal relationships present among the distinct phenotypes of peanut-reactive T cells. Analysis of the TCR repertoires of the six T-helper subtypes showed that most clones were primarily associated with a single subtype, indicating that these populations represent distinct clonal lineages (**Figure** 4C). We did, however, observe overlapping clones between the Th1-conv and Th17 states as well as the Tfh1-like and Tfh2-like states, suggesting that cells may transition

between these pairs of phenotypic states, or that these states may include shared cellular lineages that differentiated relatively late (46).

To determine to what extent this association between clonotype and phenotype might be influenced by epitope recognition, we next assessed whether or not TCRs showed evidence of convergence within T helper subtypes using TCRdist, a quantitative metric for similarity between a pair of TCR sequences (47) (**Methods**). A pair of cells with very similar TCR sequences may share epitope binding properties despite having different ancestries, allowing an assessment of the role of epitope recognition in shaping T cell phenotypes. We found that pairs of cells with highly similar TCRβ sequences (TCRdist < 9) had a significantly increased likelihood of both cells belonging to the same T helper subtype ($p<0.05$ by a chi-squared proportion test), with the exception of cells in the Th2A-like and Th2reg-like subtypes (**Figure** 4E). This result indicates a convergence onto common TCR motifs within most subtypes and suggests that factors such as TCR affinity or antigen context during priming (e.g. local tissue environment) may influence the induction of specific T helper phenotypes within an individual (48–50).

OIT suppresses Th2 and Th1 signatures in conventional effector, but not Tfh-like, cells. We next assessed the impact of OIT on the TCR repertoire and the identified T helper subtypes. The majority of expanded CD154+ and CD137+ clonotypes were present at three or all four of the timepoints, and no timepoint was associated with the depletion or emergence of unique expanded clonotypes or singletons, suggesting that OIT does not induce strong changes in the TCR repertoires of peanut-reactive CD154+ or CD137+ cells from peripheral blood (**Supplementary Figure** 12). Next, we evaluated phenotypic changes within peanut-reactive Th1, Th2, and Th17 clones during OIT by assessing the mean expression of their respective modules over time in each patient. Each set of Th clones was defined as all clonotypes in which the relevant module (e.g. Th2) was expressed in at least one cell at any timepoint; this definition allowed us

to include peanut-reactive T cells that may gain or lose Th gene expression as a result of OIT (**Methods**). We found evidence of suppression in Th2 and, to a lesser extent, Th1 clones (adjusted p-values of 0.036 and 0.117, respectively) between the baseline and maintenance timepoints (**Figure** 5A). This trend was not observed in patients treated with placebo (**Supplementary Figure** 13B).

To examine which of the previously defined six T helper subtypes were associated with this Th2 and Th1 suppression, we next assigned each Th1, Th2, and Th17 clonotype to the T helper subtype in which it most frequently appeared. We then quantified changes in gene module expression within each individual clonotype, an analysis that allowed us to track the phenotypes of hundreds of individual clonal lineages over the course of treatment. As a way to measure the stability of module expression over time within each clonotype, we calculated its "fractional clonal expression": the proportion of cells that expressed the corresponding module (Th2, Th1, or Th17) at each timepoint (**Methods**). From this analysis, we found that Th1-conv and Th2A-like clonotypes exhibited suppression of Th1 and Th2 genes, respectively, at the maintenance timepoint compared to baseline. This suppression was consistent with an anergic state, characterized by decreased cytokine expression in response to stimulation, and was not detected in the placebo group (**Supplementary Figure** 13C). In contrast, we did not observe statistically significant changes in module expression at the clonotype-level in the Tfh1-like, Tfh2-like, Th2reg-like, or Th17 subsets (**Figure** 5B), suggesting that these populations are more refractory to modulation by OIT than Th1-conv and Th2A-like clonotypes. A lack of suppression of Th2A-like clonotypes at maintenance was associated with poor outcome (Spearman's rho of 0.74 and p-value of 0.02), and the degree of suppression was similar between patients that achieved partial and full tolerance (**Figure** 5C). No statistically significant association between clinical outcome and degree of suppression was found in Tfh2-like clonotypes or Th1-conv clonotypes (**Supplementary Figure** 13A).

Non-Th2 inflammatory pathways at baseline are associated with clinical outcome. While a lack of Th2 suppression during OIT was associated with poor clinical outcome, the baseline expression of Th2 signatures was not predictive. To analyze immune signatures present at the beginning of treatment, we performed PCA on gene module scores of all CD154+ cells at baseline. This approach allowed us to assess major axes of phenotypic variation among CD154+ cells at baseline and investigate whether any of these axes correlated with clinical outcome. We found a striking separation by outcome at all timepoints in the scores of the first principal component (PC1) alone, with high PC1 scores associated with poor clinical outcome (**Figure** 5D). The top gene modules enriched in PC1 were defined by markers of T cell activation and effector response such as OX40, OX40L, Th17 function, STAT1, and GPR15 (**Figure** 5E; **Supplementary Figure** 14). To investigate the cell types associated with this signature, we summarized PC1 scores and module expression in the six previously identified Th subtypes. Of these, Th1-conv and Th17 cells expressed the highest levels of PC1 (**Supplementary Figure** 15). Consistent with this observation, the frequencies of Th1-conv and Th17, but not Th2, cells were also lower in the CD154+ compartment of patients with favorable clinical outcome (**Supplementary Figure** 9A). Interestingly, CD154+ cells not classified within any of the canonical CD4 T cell subtypes also showed outcome-dependent expression of modules associated with PC1 (**Supplementary Figure** 16). These results indicate that a range of CD4+ T cell phenotypes and inflammatory pathways may impact the likelihood of favorable responses to OIT.

Treg phenotypes are not significantly modulated by OIT. Tregs have been described in some studies as a correlate of favorable clinical outcome in OIT (19, 20). While we detected a strong and sustained expression of Treg markers among peanut-reactive CD137+ cells, we observed a moderate decrease in the frequency of CD137+ cells over the course of OIT (**Figure** 1C). In addition, although *IL10* in Treg module-expressing clones (gene module 1) was slightly elevated

during the buildup phase of treatment, there was not a sustained increase in the expression of the Treg module, *FOXP3*, or *IL10* among these cells over OIT (**Figure** 6A). Moreover, expression of either *IL10* or *FOXP3* did not correlate with clinical outcome. Unsupervised analysis of Treg module-expressing cells revealed three distinct subsets of Treg cells, including conventional Tregs, Tfh-like Tregs, and CCR7+ Tregs, which differed in their expression of *IL10*, *IL2RA*, and several costimulatory and memory markers (**Figure** 6, B and C). For example, Tfh-like Tregs were responsible for nearly all expression of *IL10*. No Treg cluster showed a sustained increase of *FOXP3*, *IL10*, or the Treg gene module as a result of OIT (**Figure** 6D). Finally, we did not see evidence for the induction of new peanut-reactive Treg clonotypes during OIT, as TCR repertoires of CD137+ cells remained stable over time (**Supplementary Figure** 12). Our data suggest a lack of induction of peanut-reactive Tregs during OIT, both by gene expression levels and by clonotype frequencies.

Discussion

In this study, we characterized peanut-reactive T helper cells from allergic patients undergoing OIT using single-cell RNA sequencing with paired TCR sequencing. These methods allowed us to identify patterns of expansion and TCR convergence among distinct peanut-reactive T helper subtypes and to longitudinally profile individual clonotypes throughout OIT. We found differential effects of OIT on distinct T helper subtypes, and a significant association at baseline between T cell phenotypes and clinical outcome, that was unmodulated by OIT. Our results add refinement to the transcriptomic-scale definitions of previously described subsets, reveal how clonotypes from these populations are affected during OIT, and provide additional insight into the substantial heterogeneity of peanut allergic patients.

Among sorted CD154+ and CD137+ T helper cells, we identified six subtypes of highly clonal peanut-reactive T helper cells with Th1, Th2, and Th17 signatures. Of these subtypes, the Th2A-like, Tfh2-like, and Th2reg-like cells correspond well to the previously described Th2A, Tfh13, and deviated Treg populations in food allergy (7–9, 40). We show here for the first time that these subsets have distinct TCR repertoires and that some are enriched in highly similar TCR sequences. Our results add resolution to a previous study showing that distinct repertoires exist between CD154+ and CD137+ cells (29). This segregation of TCR repertoires strongly suggests that the subsets represent distinct lineages rather than transient phenotypes, and the phenomenon of TCR convergence hints at the skewing of T cell state due to epitope interactions or epitope-associated factors (50–52). We did not detect significant TCR convergence in the Th2A-like and the Th2reg-like subsets, which could be due to the higher diversities of repertoires in these subsets that would require deeper sampling to detect any convergence.

Globally, we found that OIT induced a reduction of the frequency of CD154+ and CD137+ T cells and the expression of Th2 signatures in response to peanut antigen stimulation. In addition, we

found that the TCR repertoires of peanut-reactive cells in peripheral blood were stable over time. These observations suggest that OIT acts predominantly via suppression of functional phenotypes rather than by clonal deletion or TCR-biased sequestration away from the periphery. This result corroborates two previous studies that reported the emergence of anergic signatures in peanut-specific T cells over time in OIT, and provides insight into previous reports of decreases in circulating Th2 frequency following OIT (7, 17, 18, 21, 22). Nevertheless, future studies with comparatively deeper sequencing approaches and larger cohorts could further refine these observations of the influence of OIT on the peanut-reactive TCR repertoire in peripheral blood as well as among tissue resident populations.

We also showed how the six subsets of Th1, Th2, and Th17 cells identified in this study responded over the course of OIT. We observed OIT-induced suppression of Th2 and Th1 gene modules among Th2A-like and Th1-conv, but not Tfh-like, clonotypes. Strikingly, we found that the expression of select cytokines among Tfh2-like cells, but not Th2A-like cells, was correlated with peanut-specific IgE levels, suggesting that this subset may directly influence the peanut-specific IgE response. Lastly, we observed that the suppression of Th2 module expression in Th2A-like clonotypes was associated with clinical outcome. Our findings indicate that OIT modulates only a subset of peanut-reactive T cells, and that the T cells most responsible for Ig class-switching and B cell help may be the least altered by treatment, highlighting the difficulty of achieving a sustained beneficial clinical outcome.

With respect to therapeutic outcomes, we found that an unsupervised composite score of all gene modules, derived using only data from cells isolated before treatment (baseline), corresponded strongly with treatment failure and was not modulated by OIT. This score was driven largely by markers of T cell activation such as *OX40, OX40L*, and *STAT1*, as well as Th1 and Th17 genes (**Supplementary Figure** 14C). We surmise that high levels of baseline T cell activation could limit

the effectiveness of OIT due to increased inflammation or altered gastrointestinal permeability (potentially triggered by Th17 responses) (53). Assessments of genomic or immunologic features associated with clinical outcomes in OIT are scarce, but Th17 cells have been reported to play a role in atopic disease, with some preliminary evidence suggesting that they are modulated by OIT (25, 54–56). Similarly, OX40 and OX40L have also been implicated in atopic dermatitis and asthma, and represent a possible therapeutic target (57, 58).

Moreover, while some of the top gene modules in the composite score were highly enriched among Th1 and Th17 subsets (e.g., the OX40L module), many were also expressed in other compartments of CD154+ or CD137+ cells (**Supplementary Figure** 16), including CD154+ cells not classified as any of the Th subtypes. This was the case for the GPR15 and STAT1 signaling modules (**Supplementary Figure** 16B). GPR15 has been highlighted as an esophagus-homing and colon-homing receptor in CD4+ T cells (42, 59), and STAT1 (along with GBP4 and GBP1, also included in the same module) is associated with response to interferon (60, 61). Taken together, these results suggest that altered gastrointestinal permeability and inflammatory responses in diverse populations of peanut-reactive T cells may influence the likelihood of responding favorably to OIT.

While Tregs have been described by others as a correlate of favorable clinical outcome in peanut OIT (19, 20), we did not find evidence for sustained peanut-reactive Treg induction during treatment. We observed a lack of significant Treg induction both by clonotype frequency and by Treg gene expression levels, and we were able to assess this phenomenon within multiple Treg cell subtypes. Discrepancies between our results and those of prior studies could reflect differences in stimulation conditions and strategies for identifying antigen-specific Tregs (19). These differences motivate further efforts towards elucidating the role of peanut-reactive Tregs in OIT.

Here, we analyzed peanut-reactive CD4+ T cells obtained from peripheral blood. A substantial fraction of peanut-reactive T cells is likely to establish residency in tissues, including the gastrointestinal tract and lymphoid organs, but samples from these tissues cannot be as easily obtained. Thus, the impact of OIT on the phenotype and repertoire of tissue-resident peanut reactive T cells remains unexplored by this study. Despite this limitation, the study of peripheral peanut-reactive T cells during OIT has considerable translational value, as changes in the peripheral blood can be easily monitored in a clinical setting. Moreover, we and others have successfully identified clinically relevant response in peanut-reactive T cells from peripheral blood during OIT, as is shown here and in the literature (17, 22, 62).

The methods we used in this study combined FACS-based enrichment of antigen-activated T cells with single-cell RNA-Seq and TCR sequencing as a framework for profiling antigen-reactive T cells without the use of tetramer reagents. By enriching peanut-reactive T cells based on CD154 and CD137 expression, it is likely that our data included some fraction of non-specifically activated T cells. By integrating data on TCR sequences, however, we identified T cell states that were associated with clonally expanded, peanut-reactive T cells, thereby minimizing the effects of non-specifically activated T cells. We believe this framework could be used to identify likely antigen-reactive T cells in other disease contexts.

We believe this work has implications for the study of human T cell biology as well as mechanistic actions of OIT. First, the methodology implemented here provides a framework for the design and analysis of paired TCR and transcriptome data of antigen-reactive T cells, and this substantial dataset of human single-cell data provides a useful reference for future studies. Using this framework, we detected significant heterogeneity within the peanut-reactive CD154+ T cell compartment and highlighted potential roles for TCR-epitope interactions in skewing T cell

phenotype. Second, our data have revealed several features of OIT that merit further investigation. Based on our data, OIT does not appear to delete peanut-reactive Th2 clones; these findings point to selective clonal suppression, rather than deletion, as a major mechanism of OIT and highlight why sustained tolerance may be difficult to achieve. Furthermore, we found that failure to respond to OIT was reflected in a broad baseline activation signature, highly expressed in Th17 and other T cells, that was resistant to modulation by OIT. In the future, prospective OIT studies could evaluate this signature as a predictor of treatment success.

In summary, we used single-cell RNA-Seq and TCR clonotyping to reveal a complex set of highly distinct peanut-reactive T helper cell phenotypes, beyond effector Th2, that are relevant to the efficacy of OIT. Future therapeutic modalities that either target these diverse phenotypes and inflammatory pathways, such as Tfh, Th17, OX40-OX40L, or that appreciably delete peanut-specific Th2A and Tfh2-like cells, may be more likely to promote sustained tolerance in food allergy than allergen-based approaches alone.

Methods

Patients. Peanut-allergic individuals age 7 years and older were enrolled in a peanut OIT trial (NCT01750879) at the Food Allergy Center at Massachusetts General Hospital. Study participants with a previous diagnosis of peanut allergy, a history of peanut-induced reactions consistent with immediate hypersensitivity, and confirmatory peanut- and Ara h 2–specific plasma IgE concentrations (peanut-specific IgE > 5 kU/L, Ara h 2–specific IgE > 0.35 kU/L; ImmunoCAP; Thermo Fisher, Waltham, MA) underwent a double-blind placebo-controlled food challenge (DBPCFC). Increasing peanut protein doses were administered every 20 minutes to a maximum dose of 300 mg according to the following schedule: 3, 10, 30, 100, and 300 mg, for a cumulative total of 443 mg. Patients who had an objective allergic reaction during the challenge were eligible for inclusion in the study. Demographic classifications were made by the participants.

Oral immunotherapy (OIT) study. The main objective of this phase I/II, double-blind placebo-controlled, interventional study was to provide safety and mechanistic data on OIT for people with IgE-mediated peanut allergy. Enrolled patients were randomized to receive either treatment (peanut flour) or placebo (roasted oat flour) at a ratio of 3:1. Treatment consisted of a modified-rush protocol, followed by a build-up phase lasting for 44 weeks or when the patient reached 4000mg, whichever came first. Treatment dose was administered daily, and dosing escalation was incremental, based on previous OIT studies (20, 26), occurring every two weeks. After the buildup phase, patients entered a maintenance phase in which treatment was continued at the top tolerated dose for each patient for 12 weeks. Finally, patients underwent an avoidance phase, 12 weeks off therapy while strictly avoiding dietary peanut protein, in order to assess the durability of any desensitization resulting from OIT. During each phase of the study, a blood sample was taken, for four samples total per patient: 2 weeks prior to the start of treatment at baseline, 14 weeks into the buildup phase, 8 weeks into the maintenance phase, and 8 weeks into the avoidance phase.

Clinical assessments were made by double-blind placebo-controlled food challenge at baseline (DBPCFC1), at the end of 12 weeks of maintenance therapy (DBPCFC2), and at the end of 12 weeks of avoidance (20) (DBPCFC3). Clinical outcomes were defined as: treatment failure (failure to achieve the minimum maintenance dose (600 mg) of peanut protein by 12 months, or an eliciting dose less than 1443 mg at DBPCFC2, or less than 443mg at DBPCFC3, OR less than 10-fold more than at DBPCFC1); partial tolerance (eliciting dose less than 4430mg at DBPCFC3 but at least 443 mg AND more than 10-fold more than at DBPCFC1); and tolerance (ingestion of 4430 mg of peanut protein at DBPCFC3 without symptoms).

Cell purification and sorting. After a blood sample was collected, PBMCs were isolated by density gradient centrifugation (Ficoll-Paque Plus; GE Healthcare) and cryopreserved in FBS with 10% DMSO. After the study was completed, for each of the 12 patients, PBMCs from all four time points (15-30 x 10^6 PBMCs per timepoint) were simultaneously thawed, washed with PBS, and cultured in AIM-V medium (Gibco) with 100 µg/ml peanut protein extract for 20h, at a density of 5 x 10^6 PBMCs in 1 mL medium per well in 24-well plates. Peanut protein extract was prepared by agitation of defatted peanut flour (Golden Peanut and Tree Nuts, Alpharetta, GA) with PBS, centrifugation, and sterile-filtering. Endotoxin concentration in the peanut protein extract was assessed to be 6 EU/mg, using a LAL Endotoxin Quantitation kit (Thermo Fisher; cat. no. 88282). This is lower than the concentration in commercially available endotoxin-depleted preparations of the purified peanut proteins Ara h 1 and Ara h 2 (Indoor Biotechnologies; LTN-AH1-1 and LTN-AH2-1). Furthermore, the endotoxin concentration in the PBMC cultures with peanut protein extract was 0.6 EU/ml, which is comparable to the endotoxin limit for eluates from medical devices (0.5 EU/ml) as determined by the FDA (63). Anti-CD154-PE antibody (BD Biosciences; clone TRAP1) was added to the cultures at a 1:50 dilution (20 µl/well) for the last 3h. After harvesting, the cells were labeled with anti-CD3-AF700 (BD Biosciences; UCHT1), anti-CD4-APC-Cy7 (BD Biosciences; RPA-T4), anti-CD45RA-PE-Cy7 (BD Biosciences; HI100), anti-CD154-PE (BD Biosciences; TRAP1), anti-CD137-APC (BD Biosciences; clone 4B4-1), and Live/Dead Fixable

Blue stain (Thermo Fisher; cat. no. L23105). Cells were then sorted with a FACSAria Fusion instrument (BD Biosciences). Cells were gated as live singlet CD3+CD4+CD45RA- and then sorted as either CD154+CD137+/- (referred to as “CD154+”), CD154-CD137+ (“CD137+”), or CD154-CD137-.

Single-cell RNA-Seq. Sorted subsets of CD4 memory T cells were processed for single-cell RNA sequencing using the Seq-Well platform as previously described (36). A portion of each cDNA library was reserved for paired TCRα/β enrichment. The rest was barcoded and amplified using the Nextera XT kit and sequenced on the Illumina NovaSeq.

Raw read processing was performed as in Macosko et al (64). Briefly, sequencing reads were aligned to the ‘hg38’ reference human genome, collapsed by unique molecular identifier (UMI), and counted to obtain a digital gene expression matrix of cells versus genes. These counts were then filtered to exclude any cells with fewer than 1000 genes or 2000 UMIs and normalized by library size per cell and a log transformation. (For the rare T helper subsets analysis which required more cells, a filter of 500 genes and 1000 UMIs was used.) After this filtering step, we recovered a total of 74,646 CD154+ cells from 12 patients, 41,186 CD137+ cells from 11 patients, and 18,297 CD154-CD137- cells from 6 patients.

Paired single-cell TCR$\alpha\beta$ sequencing. Paired TCR sequencing was performed according to Tu et al (37). Briefly, following cDNA amplification, biotinylated capture probes for human TRAC and TRBC regions were annealed to cDNA. Magnetic streptavidin beads were used to enrich the bound TCR sequences, which were then further amplified using human V-region primers and prepared for sequencing using Nextera sequencing handles. Libraries were sequenced on an Illumina MiSeq using 150bp-length reads.

TCR sequencing reads were preprocessed according to Tu et al (37). In short, reads were mapped to TCRV and TCRJ IMGT reference sequences via IgBlast, and V and J calls with “strong plurality” (wherein the ratios of the most frequent V and J calls to the second most frequent calls

were at least 0.6) were retained. CDR3 sequences were called by identifying the 104-cysteine and 118-phenylalanine according to IMGT references and translating the amino acid sequences in between those residues. Processed TCR sequences were then paired with the single-cell transcriptome data via the cell barcodes.

Visualization of single-cell RNA-Seq data. Visualization of single-cell transcriptomes was done with UMAP (65) (uniform manifold approximation and projection) with the Python package "scanpy". Prior to visualization, the normalized gene expression data was transformed using a standard "regress-out" approach to mitigate batch effects: a multiple linear regression was performed on all genes with two covariates that could be batch-associated (numbers of transcripts per cell, and percent of transcripts aligning to the mitochondrial chromosome). The residuals from this regression were taken as the transformed data. Next, a principal components analysis was performed, and the top 10 components were used to generate a UMAP visualization.

Gene module discovery. Coexpressed gene modules were generated based on a sparse PCA approach described by Witten et al and implemented in the R package "PMA" (38). This unsupervised method employs an L1 norm penalty on loadings in each component to introduce sparsity. Prior to running sparse PCA, the gene expression matrix was randomly downsampled to have an equal number of cells from all samples, to prevent the results from being skewed by a subset of the samples. Genes were filtered down to the union of immune genes (defined by the set of gene lists available on ImmPort at https://www.immport.org/shared/genelists) and the variable genes in the dataset (defined using the R package "Seurat"). Finally, the gene expression data was scaled with respect to genes, and sparse PCA was run using the command "SPC". Gene module scores were calculated as the scaled gene expression input matrix multiplied by the outputted loadings matrix "v". The first 50 gene modules were retained for downstream analysis.

Cells were classified as "expressing" or "not expressing" a module using a simple thresholding strategy. The distribution of module scores of CD154-CD137- cells was used as a negative

control, and a threshold was set at the point where 0.2% of CD154-CD137- cells were in the positive population. Cells with a module score above the threshold were labeled as “expressing” that module. Modules in which at least 60% of the expressing cells were from a single patient were removed from downstream analysis. For analysis with the Treg module (module 1), which was more highly expressed among CD154-CD137- cells than the other Th modules, we instead identified a threshold score (ModuleScore = 2.0) that most accurately separated the positive and negative populations.

Identification of T helper subtypes. All CD154+ and CD137+ cell transcriptomes were classified as Th1, Th2, or Th17 using the criteria for module expression detailed above (see **Gene module discovery**) for the Th1, Th2, and Th17 gene modules. If a cell expressed more than one Th module, it was assigned to the module with the highest z-score (compared to the distribution of all CD154+ and CD137+ cells). Then, each individual Th class (Th1, Th2, and Th17 cells) was separately visualized by UMAP and clustered by Louvain clustering using the R package ‘Seurat’. For Treg analysis, all CD154+ and CD137+ cells, including those with Th1, Th2, or Th17 signatures, were considered using the criteria for module expression in Tregs (see **Gene module discovery**).

Distance analysis of TCR sequences. Pairwise distance of TCRβ CDR3 sequences was evaluated using the TCRdist method published by Dash et al (47). Briefly, for two TCRβ CDR3 amino acid sequences of the same length, each residue position was compared, and a penalty was assessed for every mismatch. The penalty for two different amino acid residues i and j was assessed using the BLOSUM62 matrix and was defined as min(4 – BLOSUM62[i, j], 4). Each substitution thus incurred a penalty between 1 and 4. The overall distance between two CDR3s was calculated as the sum of penalties at all positions. In the case of two CDR3s of unequal length, the sequences were aligned in all possible ways and the minimum overall penalty was taken, with each gap incurring a penalty of 8.

Likelihood-based association between TCR and T helper subtype. Likelihood-based analysis was used to determine the tightness of association between T helper subset and TCRβ CDR3 sequence. A log-likelihood ratio was defined as $\log_2(P/P_0)$, where P was the probability of two cells being of the same T helper subset if they were drawn randomly from all cells sharing the same TCRβ CDR3 sequence (without replacement), and P_0 was the probability of two cells being of the same T helper subset if they were drawn randomly from all cells. P_0 represents the prior probability without the constraint of TCR information; thus, the ratio P/P_0 represents the gain in likelihood due to the knowledge of TCR sequence. This analysis was constrained to consider all pairs of cells within the same patient.

Analysis of gene module suppression in Th and Treg clones. To quantify suppression or induction of relevant Th and Treg gene and gene module expression over time, we first identified Th (Th1, 2, or 17) and Treg clones, defined as clonotypes in which the relevant module (e.g. Th2) was expressed in at least one cell at any timepoint. This approach allowed us to expand our analysis to peanut-reactive cells that may gain or lose Th or Treg phenotypes over the course of OIT. Mean expression of genes or gene modules were then calculated for each patient at each timepoint. For analysis of Treg clones, patient 105 (full tolerance) was omitted since data from CD137+ T cells was not available (see **Single-cell RNA-Seq**).

Longitudinal analysis of individual clonotypes. Temporal analysis of individual clonotypes over the course of OIT involved two analyses: 1) obtaining the distribution of timepoints at which each clonotype was detected, and 2) assessing module expression of clonotypes within T helper subtypes. For the former, CD154+ or CD137+ clones were filtered to those with at least 4 cells in that sorted subset. Then, the timepoints covered by the cells were tabulated and the clonotype was classified as having a specific temporal pattern (e.g. “BL, BU, AV”). For the latter, clonotypes were filtered down to those with at least 2 cells in the combined CD154+ and CD137+ compartments at each timepoint. Each clonotype was then assigned to one of the six T helper

subtypes (or no subtype) based on the most frequent T subtype that its cells mapped to (see **Identification of T helper subtypes**). At each timepoint, the fraction of cells within each clonotype expressing the relevant module (Th1, Th2, or Th17) was counted, relative to the total number of cells of that clonotype at that timepoint. Fractional expression was used instead of module scores to normalize for clonotype- or patient-driven differences in dynamic range of module expression.

Baseline signature of all modules using PCA. Principal component analysis was used to identify broad immune signatures associated with clinical outcome. Mean module scores of the 50 gene modules (minus the 7 modules associated with a single patient; see **Gene module discovery**) were computed for each patient at each timepoint. Averages at baseline were used to compute the principal components. The first principal component ("PC1"), or the component explaining the largest amount of variance, was then applied to module averages of other timepoints.

Spearman correlation of treatment outcome and module expression. To investigate whether treatment outcome was correlated with expression of modules enriched in PC1, we assigned numerical values to each of the outcomes (TO as 2, PT as 1, and TF as 0) to represent an ordinal relationship between the outcomes. Spearman correlation between mean module expression (by patient and cell subset) and outcomes was calculated. Corresponding unadjusted p-values were reported.

Data availability. FASTQ file format data related to human samples will be available through dbGaP under accession number phs001897.v2.p1. Processed gene expression and associated TCR clonotype data will be available through GEO under accession number GSE158667. Processed data files and associated meta data tables for Figures 1-6 will be made available on https://github.com/mitlovelab/, under GSE158667, or upon request.

Code availability. R, python, and Matlab scripts for processing TCR sequencing data and generating all analyses, as well as all updates, will be made available on https://github.com/mitlovelab or upon request.

Statistics. All statistical tests were performed as two-sided tests unless otherwise noted. The statistical tests used in each figure are indicated in the respective figure legend. Box plots were plotted with the standard visualization of 25^{th} and 75^{th} percentile for the lower and upper hinges, and at most 1.5 times the interquartile range for the whisker lengths. P-values less than 0.05 were considered statistically significant. All Wilcoxon rank-sum analyses were two-sided unless stated otherwise. All adjusted p-values were calculated using Bonferroni correction unless stated otherwise.

Study approval. All subjects were recruited with informed consent, and the study was approved by the Institutional Review Board of Mass General Brigham Healthcare (protocol 2012P002153).

Author Contributions

W.G.S. and J.C.L. conceptualized the study. W.G.S. conducted the clinical trial (NCT01750879). B.M., A.A.T., B.R., and P.M.P. conducted experiments. B.M., A.A.T., D.M.M., and N.P.S. analyzed the data. T.M.G. and J.H.G. conducted experiments to develop and validate methods. B.M., A.A.T., B.R., D.M.M., W.G.S., and J.C.L. wrote and edited the manuscript. B.M. and A.A.T. contributed equally to this research as co-first authors. The order of appearance of the co-first authors was based on the timeline of contributions to the work.

Acknowledgements

We would like to thank our patients and their families who generously gave their time and participation, as well as Lauren Tracy, Colby Rondeau, Christine Elliot and Leah Hayden, the clinical coordinators of this study. We would also like to thank Sarita U. Patil and Yamini V. Virkud for fruitful discussions. The clinical work was performed in the Harvard Clinical and Translational

Science Center supported by grants 1UL1TR001102 and 8UL1TR000170 from the National Center for Advancing Translational Sciences, and 1UL1RR025758 from the National Center for Research Resources. In addition, we thank our colleagues at the MGH Department of Pathology Flow and Image Cytometry Research Core for their help with cell sorting. The Flow Core obtained funding from the National Institutes of Health Shared Instrumentation program (1S10OD012027-01A1, 1S10OD016372-01, 1S10RR020936-01, and 1S10RR023440-01A1). This work was supported in part by the Koch Institute Support (core) NIH Grant P30-CA14051 from the National Cancer Institute, as well as the Koch Institute - Dana-Farber/Harvard Cancer Center Bridge Project. This work was also supported by the Food Allergy Science Initiative at the Broad Institute and the NIH (5P01AI039671, 5U19AI089992, U19AI095261).

References

1. Patil SU, et al. Peanut oral immunotherapy transiently expands circulating Ara h 2–specific B cells with a homologous repertoire in unrelated subjects. *J Allergy Clin Immunol*. 2015;136(1):125-134.e12.
2. Sicherer SH and Sampson HA. Food allergy: A review and update on epidemiology, pathogenesis, diagnosis, prevention, and management. *J Allergy Clin Immunol*. 2018;141(1):41-58.
3. Gupta RS, et al. The prevalence, severity, and distribution of childhood food allergy in the United States. *Pediatrics*. 2011;128(1).
4. Vickery BP, et al. Pathophysiology of Food Allergy. *Pediatr Clin North Am*. 2011;58(2):363-376.
5. Prussin C, et al. TH2 heterogeneity: Does function follow form? *J Allergy Clin Immunol*. 2010;126(6):1094-1098.
6. Sampath V and Nadeau KC. Newly identified T cell subsets in mechanistic studies of food immunotherapy. *J Clin Invest*. 2019;129(4):1431-1440.
7. Wambre E, et al. A phenotypically and functionally distinct human TH2 cell subpopulation is associated with allergic disorders. *Sci Transl Med*. 2017;9(401):eaam9171.
8. Gowthaman U, et al. Identification of a T follicular helper cell subset that drives anaphylactic IgE. *Science (80-)*. 2019;365(6456):eaaw6433.
9. Mitson-Salazar A, et al. Hematopoietic prostaglandin D synthase defines a proeosinophilic pathogenic effector human T H 2 cell subpopulation with enhanced function. *J Allergy Clin Immunol*. 2016;137(3):907-918.e9.
10. Ruiter B, et al. Expansion of the CD4+ effector T-cell repertoire characterizes peanut-allergic patients with heightened clinical sensitivity. *J Allergy Clin Immunol*. 2020;145(1):270-282.
11. Vickery BP, et al. AR101 Oral Immunotherapy for Peanut Allergy. *N Engl J Med*.

2018;379(21):1991-2001.

12. Chinthrajah RS, et al. Sustained outcomes in oral immunotherapy for peanut allergy (POISED study): a large, randomised, double-blind, placebo-controlled, phase 2 study. *Lancet*. 2019;394(10207):1437-1449.

13. Blumchen K, et al. Oral peanut immunotherapy in children with peanut anaphylaxis. *J Allergy Clin Immunol*. 2010;126(1):83-91.e1.

14. Vickery BP, et al. Sustained unresponsiveness to peanut in subjects who have completed peanut oral immunotherapy. *J Allergy Clin Immunol*. 2014;133(2):468-475.e6.

15. Blumchen K, et al. Efficacy, Safety, and Quality of Life in a Multicenter, Randomized, Placebo-Controlled Trial of Low-Dose Peanut Oral Immunotherapy in Children with Peanut Allergy. *J Allergy Clin Immunol Pract*. 2019;7(2):479-491.e10.

16. Kim EH, et al. Sublingual immunotherapy for peanut allergy: clinical and immunologic evidence of desensitization. *J Allergy Clin Immunol*. 2011;127(3):640-6.e1.

17. Ryan JF, et al. Successful immunotherapy induces previously unidentified allergen-specific CD4+ T-cell subsets. *Proc Natl Acad Sci U S A*. 2016;113(9):E1286-E1295.

18. Frischmeyer-Guerrerio PA, et al. Mechanistic correlates of clinical responses to omalizumab in the setting of oral immunotherapy for milk allergy. *J Allergy Clin Immunol*. 2017;140(4):1043-1053.e8.

19. Syed A, et al. Peanut oral immunotherapy results in increased antigen-induced regulatory T-cell function and hypomethylation of forkhead box protein 3 (FOXP3). *J Allergy Clin Immunol*. 2014;133(2):500-510.e11.

20. Varshney P, et al. A randomized controlled study of peanut oral immunotherapy: Clinical desensitization and modulation of the allergic response. *J Allergy Clin Immunol*. 2011;127(3):654-660.

21. Weissler KA, et al. Identification and analysis of peanut-specific effector T and regulatory T cells in children allergic and tolerant to peanut. *J Allergy Clin Immunol*.

2018;141(5):1699-1710.e7.

22. Wang W, et al. Transcriptional changes in peanut-specific CD4+ T cells over the course of oral immunotherapy. *Clin Immunol*. 2020;219(March):108568.

23. Wambre E. Effect of allergen-specific immunotherapy on CD4+ T cells. *Curr Opin Allergy Clin Immunol*. 2015;15(6):581-587.

24. Tordesillas L and Berin MC. Mechanisms of Oral Tolerance. *Clin Rev Allergy Immunol*. 2018;55(2):107-117.

25. Chiang D, et al. Single-cell profiling of peanut-responsive T cells in patients with peanut allergy reveals heterogeneous effector TH2 subsets. *J Allergy Clin Immunol*. 2018;141(6):2107-2120.

26. Jones SM, et al. Clinical efficacy and immune regulation with peanut oral immunotherapy. *J Allergy Clin Immunol*. 2009;124(2).

27. Chattopadhyay PK, et al. A live-cell assay to detect antigen-specific CD4+ T cells with diverse cytokine profiles. *Nat Med*. 2005;11(10):1113-1117.

28. Chattopadhyay PK, et al. Live-cell assay to detect antigen-specific CD4+ T-cell responses by CD154 expression. *Nat Protoc*. 2006;1(1):1-6.

29. Bacher P, et al. Regulatory T Cell Specificity Directs Tolerance versus Allergy against Aeroantigens in Humans. *Cell*. 2016;167(4):1067-1078.e16.

30. Aguet F, et al. Genetic effects on gene expression across human tissues. *Nature*. 2017;550(7675):204-213.

31. Liu K, et al. Augmentation in Expression of Activation-Induced Genes Differentiates Memory from Naive CD4 + T Cells and Is a Molecular Mechanism for Enhanced Cellular Response of Memory CD4 + T Cells . *J Immunol*. 2001;166(12):7335-7344.

32. Kunnath-Velayudhan S, et al. Transcriptome Analysis of Mycobacteria-Specific CD4 + T Cells Identified by Activation-Induced Expression of CD154. *J Immunol*. 2017;199(7):2596-2606.

730 33. Commandeur S, et al. Clonal Analysis of the T-Cell Response to In Vivo Expressed
731 Mycobacterium tuberculosis Protein Rv2034, Using a CD154 Expression Based T-Cell
732 Cloning Method. Scriba TJ, ed. *PLoS One*. 2014;9(6):e99203.
733 34. Huang H, et al. Analyzing the Mycobacterium tuberculosis immune response by T-cell
734 receptor clustering with GLIPH2 and genome-wide antigen screening. *Nat Biotechnol*.
735 Published online April 27, 2020:1-9.
736 35. Smith NP, et al. Identification of antigen-specific TCR sequences based on biological and
737 statistical enrichment in unselected individuals. *JCI Insight*. 2021;6(13).
738 36. Gierahn TM, et al. Seq-Well: portable, low-cost RNA sequencing of single cells at high
739 throughput. *Nat Methods*. 2017;14(4):395-398.
740 37. Tu AA, et al. TCR sequencing paired with massively parallel 3′ RNA-seq reveals
741 clonotypic T cell signatures. *Nat Immunol*. 2019;20(12):1692-1699.
742 38. Witten DM, et al. A penalized matrix decomposition, with applications to sparse principal
743 components and canonical correlation analysis. *Biostatistics*. 2009;10(3):515-534.
744 39. Kim CJ, et al. The Transcription Factor Ets1 Suppresses T Follicular Helper Type 2 Cell
745 Differentiation to Halt the Onset of Systemic Lupus Erythematosus. *Immunity*.
746 2018;49(6):1034-1048.e8.
747 40. NovalRivas M, et al. Regulatory T cell reprogramming toward a Th2-Cell-like lineage
748 impairs oral tolerance and promotes food allergy. *Immunity*. 2015;42(3):512-523.
749 41. Velu V, et al. Induction of Th1-Biased T Follicular Helper (Tfh) Cells in Lymphoid Tissues
750 during Chronic Simian Immunodeficiency Virus Infection Defines Functionally Distinct
751 Germinal Center Tfh Cells. *J Immunol*. 2016;197(5):1832-1842.
752 42. Morgan DM, et al. Clonally expanded, GPR15-expressing pathogenic effector Th2 cells
753 are associated with eosinophilic esophagitis. *Sci Immunol*. 2021;6(62).
754 43. Sonoda E, et al. Transforming growth factor beta induces IgA production and acts
755 additively with interleukin 5 for IgA production. *J Exp Med*. 1989;170(4):1415-1420.

44. RL C, et al. Transforming growth factor beta specifically enhances IgA production by lipopolysaccharide-stimulated murine B lymphocytes. *J Exp Med*. 1989;170(3):1039-1044.
45. Seumois G, et al. Single-cell transcriptomic analysis of allergen-specific T cells in allergy and asthma. *Sci Immunol*. 2020;5(48):eaba6087.
46. James KR, et al. Distinct microbial and immune niches of the human colon. *Nat Immunol*. 2020;21(3):343-353.
47. Dash P, et al. Quantifiable predictive features define epitope-specific T cell receptor repertoires. *Nature*. 2017;547(7661):89-93.
48. Hayes SM, et al. TCR signal strength influences αβ/γδ lineage fate. *Immunity*. 2005;22(5):583-593.
49. Daniels MA and Teixeiro E. TCR Signaling in T Cell Memory. *Front Immunol*. 2015;6(DEC):617.
50. Snook JP, et al. TCR signal strength controls the differentiation of CD4+ effector and memory T cells. *Sci Immunol*. 2018;3(25).
51. Tubo NJ, et al. Single naive CD4+ T cells from a diverse repertoire produce different effector cell types during infection. *Cell*. 2013;153(4):785-796.
52. Kotov DI, et al. TCR Affinity Biases Th Cell Differentiation by Regulating CD25, Eef1e1, and Gbp2. *J Immunol*. 2019;202(9):2535-2545.
53. Stockinger B and Omenetti S. The dichotomous nature of T helper 17 cells. *Nat Rev Immunol*. 2017;17(9):535-544.
54. Choy DF, et al. TH2 and TH17 inflammatory pathways are reciprocally regulated in asthma. *Sci Transl Med*. 2015;7(301):301ra129.
55. Hirahara K and Nakayama T. CD4+ T-cell subsets in inflammatory diseases: Beyond the Th1/Th2 paradigm. *Int Immunol*. 2016;28(4):163-171.
56. Luce S, et al. Th2A and Th17 cell frequencies and regulatory markers as follow-up

biomarker candidates for successful multifood oral immunotherapy. *Allergy*. 2020;75(6):1513-1516.

57. Guttman-Yassky E, et al. GBR 830, an anti-OX40, improves skin gene signatures and clinical scores in patients with atopic dermatitis. *J Allergy Clin Immunol*. 2019;144(2):482-493.e7.

58. Seshasayee D, et al. In vivo blockade of OX40 ligand inhibits thymic stromal lymphopoietin driven atopic inflammation. *J Clin Invest*. 2007;117(12):3868-3878.

59. Habtezion A, et al. Leukocyte trafficking to the small intestine and colon. *Gastroenterology*. 2016;150(2):340-354.

60. Adamczyk A, et al. Differential expression of GPR15 on T cells during ulcerative colitis. *JCI insight*. 2017;2(8).

61. Ovadia A, et al. Two different STAT1 gain-of-function mutations lead to diverse IFN-γ-mediated gene expression. *npj Genomic Med*. 2018;3(1):23.

62. Manohar M, et al. Immune changes beyond Th2 pathways during rapid multifood immunotherapy enabled with omalizumab. *Allergy*. Published online May 29, 2021:all.14833.

63. Guidance for Industry: Pyrogen and Endotoxins Testing: Questions and Answers | FDA.

64. Macosko EZ, et al. Highly Parallel Genome-wide Expression Profiling of Individual Cells Using Nanoliter Droplets. *Cell*. 2015;161(5):1202-1214.

65. McInnes L, et al. UMAP: Uniform Manifold Approximation and Projection for Dimension Reduction. arXiv:1802.03426. Posted on arXiv February 9, 2018.

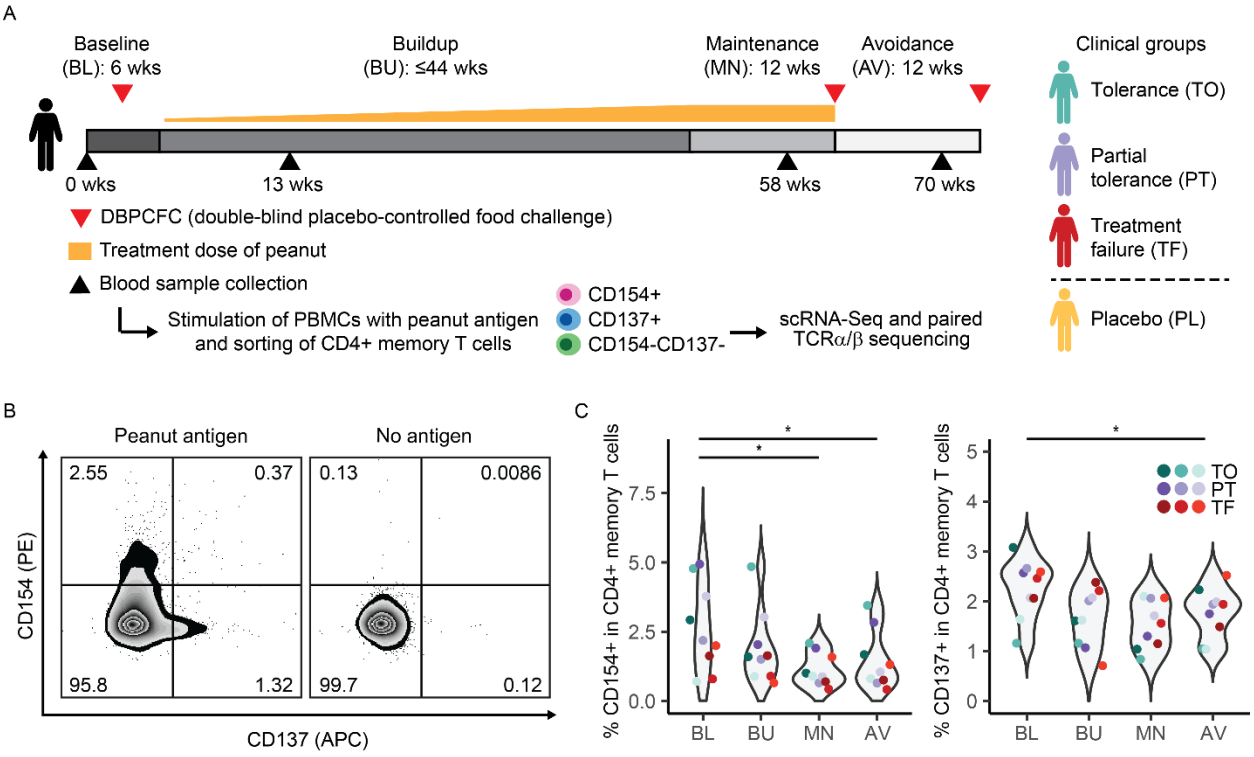

Figure 1. Peanut-reactive T cells decrease in frequency over the course of OIT. A, OIT study design, sample processing, and patient cohorts. CD3+CD4+CD45RA- memory T cells were sorted by FACS as CD154+CD137+/- ("CD154+"), CD154-CD137+ ("CD137+"), or CD154-CD137-. For definition of clinical outcomes and patient information, see **Methods** and **Supplementary Tables** 1 and 2. **B**, Representative flow plots from one patient at one timepoint (n = 12 patients total). **C**, Percent of CD4+ memory T cells at each time point that are CD154+ (left) or CD137+ (right) in peanut-stimulated PBMC cultures from patients in the treatment group. '*' refers to an adjusted p-value of <0.05 by paired Wilcoxon rank-sum test.

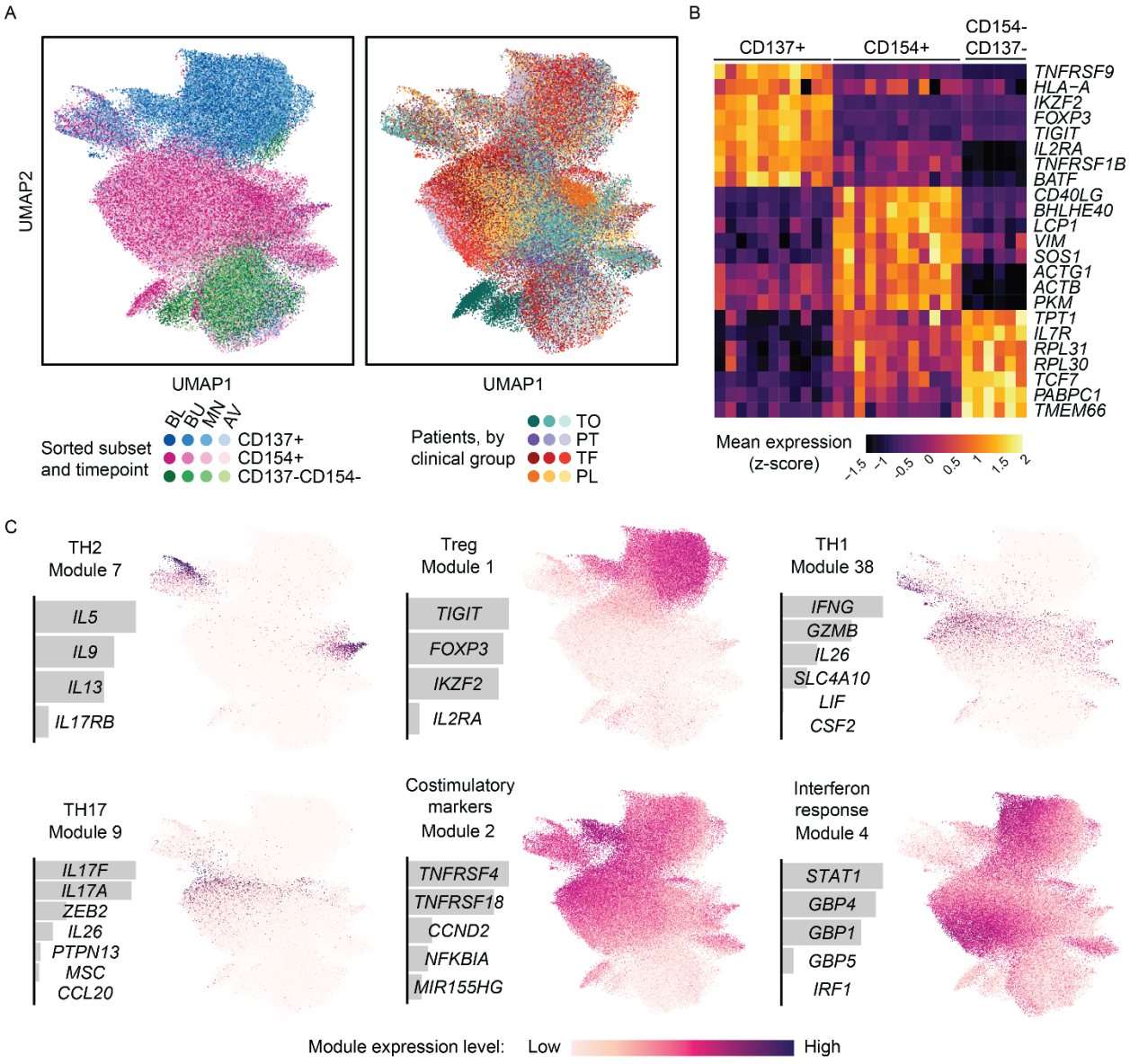

Figure 2. Peanut-reactive T cells from OIT patients have diverse and distinct transcriptional signatures. A, Two-dimensional UMAP visualization of all single-cell transcriptomes (n = 134,129 cells), colored by sorted subset and timepoint (left) or by patient and clinical group (right). **B**, Top differentially expressed genes between the sorted subsets. Each column represents the scaled average gene expression of cells from a single patient. Genes were selected using a ROC test. **C**, Selected gene modules discovered using sparse principal components analysis, labeled with module number and a proposed descriptor. For each module, the relative weights of each contributing gene and the module score of all cells overlaid on the UMAP coordinates are shown.

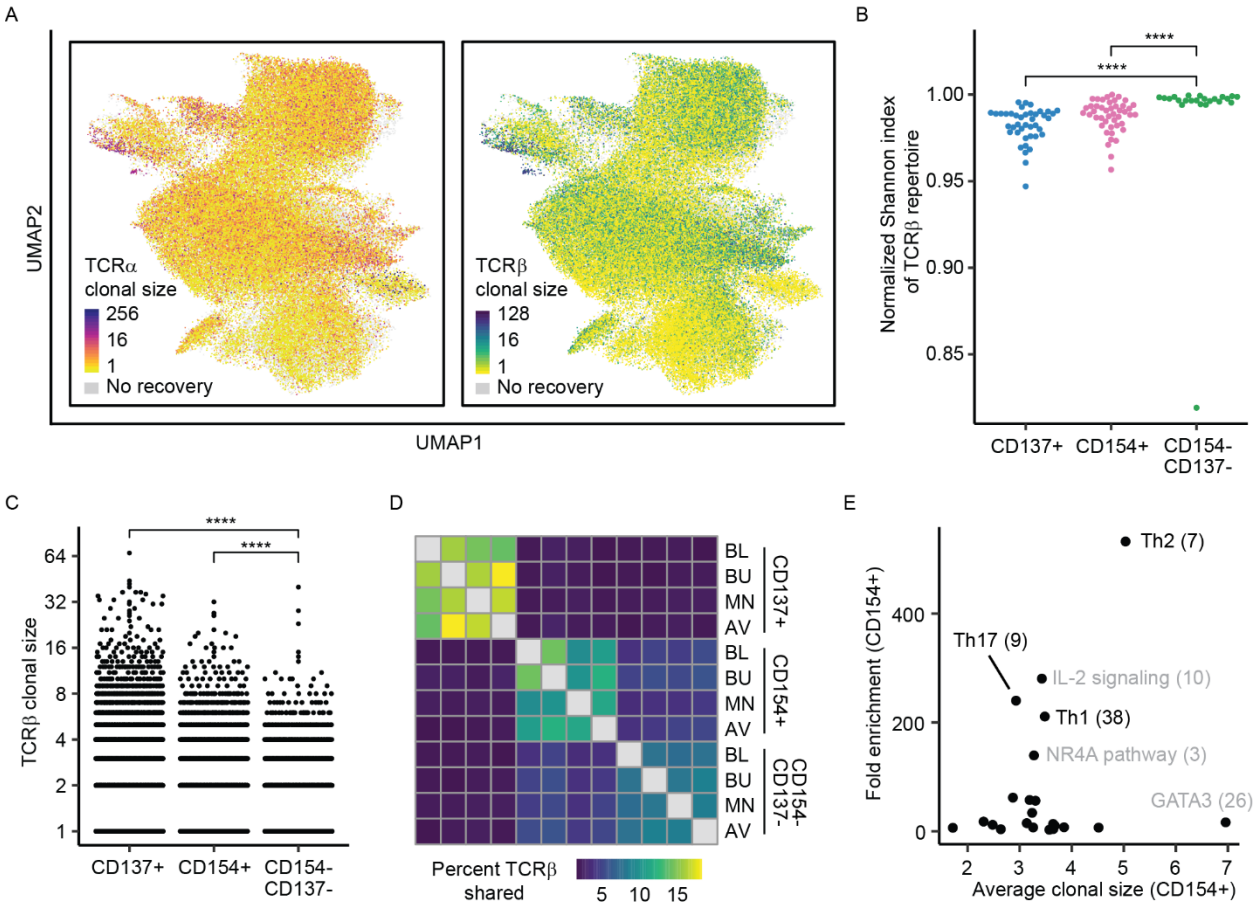

825

826 **Figure 3. Gene modules for T helper function are associated with clonal expansion and**
827 **expression in activated cells. A**, Clonal size of TCRα sequence (left) or TCRβ sequence (right)
828 for all cells with paired TCR recovery, overlaid onto UMAP coordinates. Clonal size is defined as
829 the number of cells sharing a TCR sequence. **B**, Diversity (normalized Shannon index) of TCRβ
830 repertoires of each sorted subset. Each data point represents the repertoire of one patient at one
831 time point (CD137+: n = 41; CD154+: n = 44; CD154-CD137-: n = 23). **C**, Distribution of TCRβ
832 clonal sizes, within each sorted subset. Cells within each sorted subset were downsampled to
833 equal number before clonal sizes were calculated. **D**, Percent of TCRβ sequences shared
834 between time points and sorted subsets. 'Percent shared' is defined as the number of unique
835 TCRβ sequences detected in both conditions, divided by the geometric mean of the number of
836 unique TCRβ sequences in each of the two conditions. Sequences from all patients with samples
837 in all three conditions (n = 6 patients) were pooled. **E**, Mean clonal size and fold-change in mean
838 module scores (compared to module-expressing CD154-CD137- cells) in CD154+ cells

839 expressing each gene module. Each data point represents a single gene module. Cells were
840 classified as ‘expressing’ each module or not, relative to background expression (**Methods**).
841 Clonal size was calculated with respect to all cells in the dataset. ‘****’ refers to an adjusted p-
842 value of <0.0001. Data represent combined data from all patients at all timepoints (**A**-**C,E**).

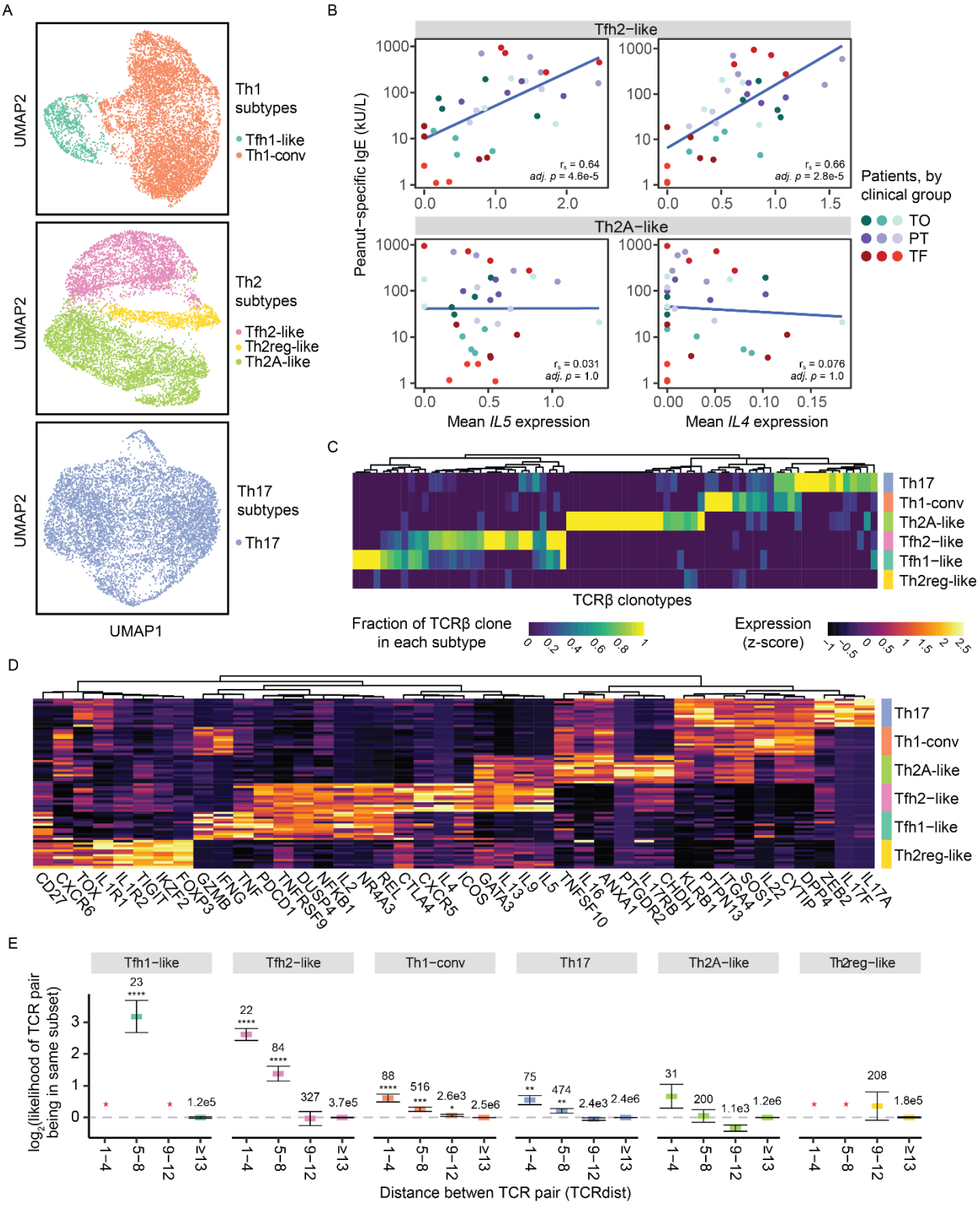

Figure 4. Peanut-reactive T helper subtypes are clonally distinct and exhibit TCR convergence. A, UMAP visualizations of Th1- (n = 7,609 cells), Th2- (n = 7,877 cells), and Th17-scoring cells (n = 7,111 cells). Clusters are annotated by their putative identity. **B,** Scatter plots of average expression of *IL5* and *IL4* in Tfh2-like cells or Th2A-like cells (within each patient at each

timepoint) and peanut-specific IgE titers. Linear fit, Spearman's correlation (r_s, n = 34), and adjusted p-values are shown. **C**, Fraction of TCRβ clonotypes belonging to each subset. Fraction is defined as the number of cells of a TCRβ CDR3 sequence (column) detected in each T helper subset, divided by the total number of cells within the clonotype. Clonotypes were randomly downsampled to visualize a comparable number from each subset. **D**, Differentially expressed genes in each T helper subset. Genes were selected using an ROC test and manual curation. Each row represents the scaled average gene expression in one patient. **E**, TCR distance analysis of TCRβ sequences. The x-axis represents bins of increasing pairwise TCR distance, calculated using TCRdist, and the y-axis represents the likelihood for pairs of cells at a given TCR distance to be of the same T helper subset, normalized to the prior probability of any two cells belonging to that subset (see **Methods**). '****' refers to an adjusted p-value of <0.0001 by a two-sided Chi-square proportion test with one degree of freedom, '***' refers to p-value of <0.001, and '**' refers to p-value of <0.01. The total number of pairs within each TCR distance and subset is indicated above each datapoint. Red '*' indicates that no TCR pair of the TCR distance was found within that subset. Error bars represent 85% binomial confidence intervals. Data represent combined data from all patients at all timepoints (**A**-**E**).

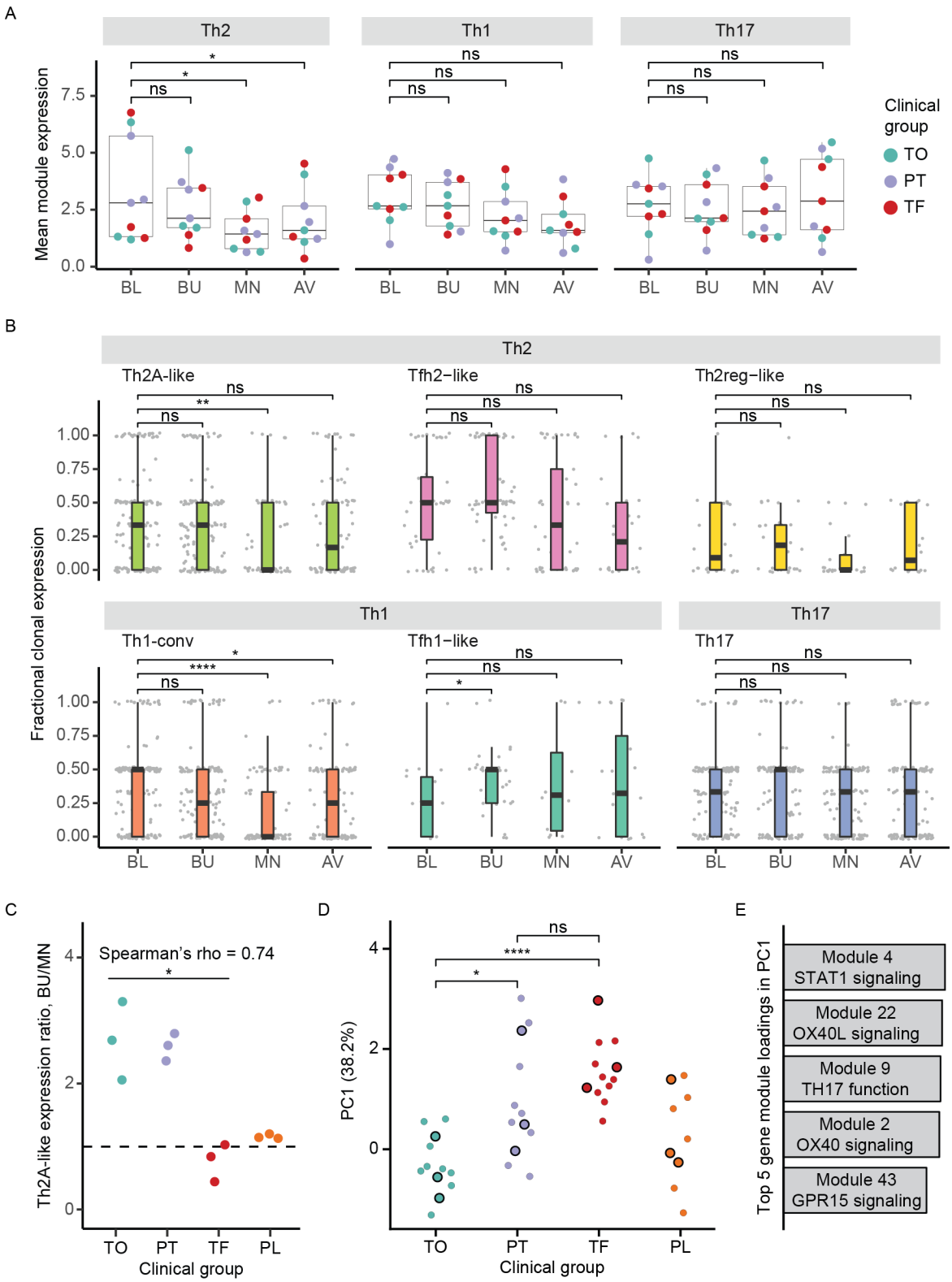

Figure 5. Th1 and Th2 effector, but not Tfh-like, subsets are suppressed by OIT. A, Mean Th2, Th1 and Th17 gene module expression over time within Th2, Th1, and Th17 clones (**Methods**), respectively, in each treatment-group patient at each timepoint. **B**, Fractional

expression of Th2, Th1, and Th17 modules within clonotypes of T helper subtypes over time. Fractional clonal expression is defined as the proportion of cells within each clonotype expressing their respective module (**Methods**). Each data point represents the cells of an individual expanded clonotype from one patient at one timepoint. Patients of the placebo group were excluded. **C**, Degree of suppression in Th2A-like clones by clinical group. Ratio of mean Th2 module expression in Th2A-like clones from each patient was calculated between buildup (BU) and maintenance (MN). Spearman's rho (n = 9) and p-value ('*' refers to p-value < 0.05) are shown Spearman correlation test between ratio and outcome within the treatment group (assigning TO as 2, PT as 1, and TF as 0). **D,** Principal component 1 (PC1) score of CD154+ cells by outcome. A principal components analysis was done using the 50 gene modules as features and all CD154+ cells at baseline as the input data (**Methods**). Each data point represents the mean PC1 score of all CD154+ cells from a single patient at a single timepoint. Black-outlined points represent the baseline timepoint. **E,** Top 5 gene module loadings in PC1. Bar heights represent the magnitude of each contribution to PC1. Further details of each gene module are available in Supplementary Figures 4 and 5. '*' refers to an adjusted p-value of <0.05 by a paired (**A**) or unpaired (**B**, **D**) Wilcoxon rank-sum test, '**' refers to adjusted p-value of <0.005, and '****' refers to adjusted p-value of <0.0005 (**A**, **B**, **D**).

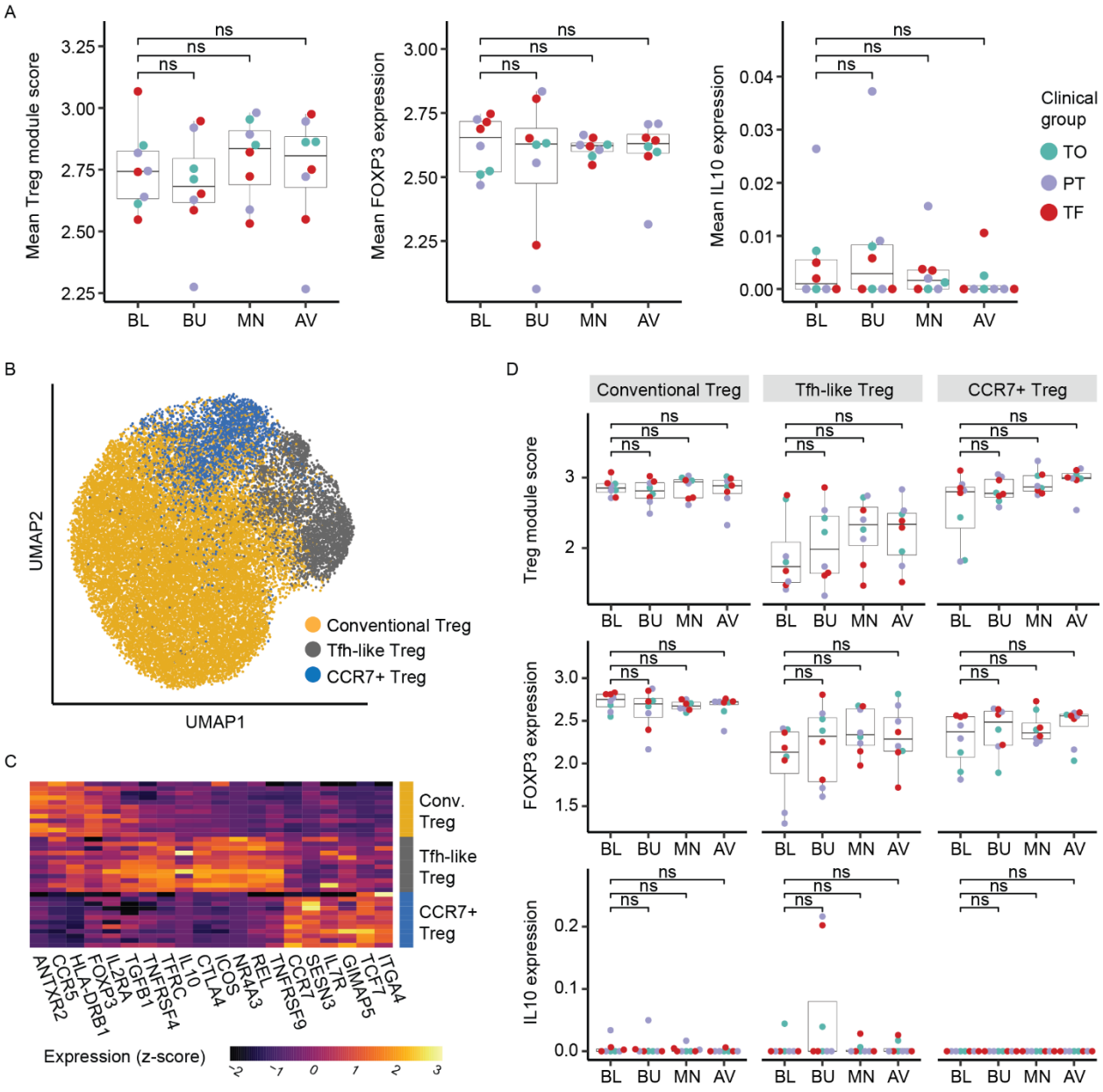

Figure 6. Treg phenotypes are not significantly modulated by OIT. A, Average expression of Treg module (gene module 1), *FOXP3*, and *IL10* by patient and timepoint within Treg clones. Each data point represents the mean expression of all Treg clone cells for a given patient at a given time point. **B**, UMAP visualization of all Treg cells (data from all patients at all timepoints), colored by cluster assignment and labeled by putative cluster identity. **C**, Differentially expressed genes in each Treg cluster. Genes were selected using an ROC test and manual curation. Each row represents the scaled average gene expression in one patient. **D**, Average expression of the Treg module (top), *FOXP3* (middle) and *IL10* (bottom) by patient and timepoint within clones of

each Treg cluster, colored by clinical group. Adjusted p-values were calculated by paired Wilcoxon rank-sum test (**A**, **D**).